PHYSICAL REVIEW D **95,** 035042 (2017)

Type II seesaw model and multilepton signatures at hadron colliders

Manimala Mitra,[1] Saurabh Niyogi,[2] and Michael Spannowsky[3]

[1]*Department of Physics, Indian Institute of Science Education and Research Mohali (IISER Mohali), Sector 81, SAS Nagar, Manauli 140306, India*

[2]*Department of Physics and Astrophysics, University of Delhi, New Delhi 110007, India*

[3]*Institute for Particle Physics Phenomenology (IPPP), Department of Physics, Durham University, Durham DH1 3LE, United Kingdom*

(Received 18 December 2016; published 28 February 2017)

We investigate multilepton signatures, arising from the decays of doubly charged and singly charged Higgs bosons in the Type II seesaw model. Depending on the vacuum expectation value of the triplet v_Δ, the doubly and singly charged Higgs bosons can decay into a large variety of multilepton final states. We explore all possible decay modes corresponding to different regimes of v_Δ that generate distinguishing four and five leptonic signatures. We focus on the 13 TeV Large Hadron Collider (LHC) and further extend the study to a very high energy proton-proton collider (VLHC) with a center-of-mass energy of 100 TeV. We find that a doubly charged Higgs boson of masses around 375 GeV can be discovered at immediate LHC runs. A heavier mass of 630 GeV can instead be discovered at the high-luminosity run of the LHC or at the VLHC with 30 fb^{-1}.

DOI: 10.1103/PhysRevD.95.035042

I. INTRODUCTION

The observation of nonzero neutrino masses and their mixings provide unambiguous experimental evidence of physics beyond the Standard Model (BSM). So far, oscillation experiments have measured the solar and atmospheric mass square differences Δm^2_{12}, $|\Delta m^2_{13}|$ and the mixing angles θ_{12}, θ_{23}, and θ_{13} [1]. Additionally, the cosmological constraints on the sum of light neutrino masses [2] bound the SM neutrinos to be less than electronvolt (eV). A natural explanation for small neutrino masses is provided by the seesaw mechanism, where eV-scale neutrino masses are generated from lepton number violating (LNV) operators of dimension five [3,4]. UV complete models generating the higher dimensional operator can have a right-handed neutrino N_R (Type I seesaw) [5–10], $SU(2)_L$ triplet Higgs Δ_L (Type II seesaw) [11–14], or a $SU(2)_L$ triplet fermionic field Σ (Type III seesaw) [15]. The Type I and Type II seesaw models can further be embedded into left-right symmetric models [16]. Another very popular model is the inverse seesaw model [17,18] where the light neutrino masses are proportional to a small LNV parameter, and thus tend to zero for a vanishingly small value of the parameter. In this model, the smallness of the neutrino mass is protected by the lepton number symmetry of the Lagrangian.[1] If we have a right-handed neutrino or Higgs triplet states with low masses (few hundreds GeV up to a few TeV), these BSM states can be directly produced at the LHC and can be detected via their decay products in direct searches [20–31]. Apart from direct production, these states may appear in loops for various processes/decays. Strong constraints can be put on doubly and singly charged scalar masses from lepton number violating processes at the LHC [32,33].[2] Another way to infer the existence of such resonances is through indirect detection experiments which also cover a wide range of masses and mixings [35].

Here we focus on the Type II seesaw mechanism. The model is augmented with a doubly charged Higgs boson that can give rise to the smoking gun signal of same-sign dilepton pairs [23–25,36]. The neutral component of the triplet Higgs develops a vacuum expectation value (VEV) v_Δ and generates neutrino masses through the Yukawa Lagrangian. In addition to the doubly charged Higgs, the model also contains a singly charged Higgs state. The details of the Higgs spectrum have been discussed in [31,37]. The particles' branching ratios and some collider signatures have been outlined in [23–25]. CMS and ATLAS have searched for pair production of doubly charged Higgs bosons, followed by their decay into same-sign dileptons and, hence, set a limit on the mass of H^{++} [38]. An alternative search where the H^{++} is produced in association with two jets was found to be less constraining [39]. Other than the dileptonic decay mode, in parts of the parameter space with relatively large triplet VEV v_Δ, the charged Higgs dominantly decays into gauge bosons or via cascade decays with on/off-shell W bosons [24,26,27]. The latter can give rise to the distinctive same-sign dilepton signatures, with additional b-jets [27].

[1]For reviews of TeV-scale seesaw models and their phenomenology see Refs. [19].

[2]For further discussion on the recent developments on muon anomalous magnetic moment and lepton flavor violation in the context of several extensions of the SM, see review [34].

In particular, the same-sign diboson scenario has been studied in the context of LHC in [40–42].

Other than the conventional channel of pair production of H^{++} that leads to four leptonic final states, one can have even up to five or six leptons via cascade decays into gauge bosons.[3] The multileptonic final states provide very clean signatures at hadron colliders. Hence, a handful of events can confirm or rule out the model. In this work, we carry out a thorough investigation on the collider search of such multilepton (four or five leptons) final states that will be useful to probe the complete range of $v_\Delta = 10^{-9}$ GeV–1 GeV. We divide this range into three regimes: small, intermediate, and large v_Δ. We focus on both the immediate run II of the LHC with 13 TeV center-of-mass energy and also its future high-luminosity upgrade (HL-LHC). We further analyze the detection prospects of such multilepton signatures at a possible future 100 TeV proton-proton collider [Very Large Hadron Collider (VLHC)] [44,45].

Our paper is organized as follows: we briefly review the basics of the Type II seesaw model in Sec. II. In Sec. III, we discuss the relevant decay modes and branching ratios. In the subsequent sections, Secs. IV and V, we analyze in detail the production cross sections and the discovery potential of the multilepton final states. Finally, we present our conclusion in Sec. VI.

II. MODEL

In this section, we briefly review the basics of the Type II seesaw scenario [11–14]. The model consists of the SM fields, with a Higgs doublet Φ and an additional $SU(2)_L$ triplet Higgs Δ that has hypercharge $U(1)_Y = 2$,

$$\Phi = \begin{pmatrix} \Phi^+ \\ \Phi^0 \end{pmatrix} \quad \text{and} \quad \Delta = \begin{pmatrix} \frac{\Delta^+}{\sqrt{2}} & \Delta^{++} \\ \Delta^0 & -\frac{\Delta^+}{\sqrt{2}} \end{pmatrix}. \tag{1}$$

The neutral components of the doublet and triplet Higgs fields are $\Phi^0 = \frac{1}{\sqrt{2}}(\phi^0 + i\chi^0)$ and $\Delta^0 = \frac{1}{\sqrt{2}}(\delta^0 + i\eta^0)$, respectively. The components ϕ^0 and δ^0 develop a VEV denoted as v_Φ and v_Δ with the light neutrino masses m_ν being proportional to the triplet VEV v_Δ. The two VEVs satisfy $v^2 = v_\Phi^2 + v_\Delta^2 = (246\ \text{GeV})^2$. The kinetic term of the new scalar field Δ that generates the interactions with the SM gauge bosons has the form

$$\mathcal{L}_{\text{kin}}(\Delta) = \text{Tr}[(D_\mu \Delta)^\dagger (D^\mu \Delta)]. \tag{2}$$

The covariant derivative of Eq. (2) is defined as

$$D_\mu \Delta = \partial_\mu \Delta + i\frac{g}{2}[\tau^a W_\mu^a, \Delta] + ig' B_\mu \Delta. \tag{3}$$

In addition, Δ also interacts with the leptons through the Yukawa interaction

$$\mathcal{L}_Y(\Phi, \Delta) = Y_\Delta \bar{L}_L^c i\tau_2 \Delta L_L + \text{H.c.} \tag{4}$$

Here, c represents the charge conjugation transformation, and Y_Δ is a 3×3 matrix. The triplet field Δ carries lepton number $+2$, and hence the Yukawa term conserves the lepton number. The scalar potential of the Higgs fields Φ and Δ is

$$\begin{aligned} V(\Phi, \Delta) = {} & m_\Phi^2 \Phi^\dagger \Phi + \tilde{M}_\Delta^2 \text{Tr}(\Delta^\dagger \Delta) + (\mu \Phi^T i\tau_2 \Delta^\dagger \Phi + \text{H.c.}) \\ & + \frac{\lambda}{4}(\Phi^\dagger \Phi)^2 + \lambda_1 (\Phi^\dagger \Phi)\text{Tr}(\Delta^\dagger \Delta) + \lambda_2 [\text{Tr}(\Delta^\dagger \Delta)]^2 \\ & + \lambda_3 \text{Tr}[(\Delta^\dagger \Delta)^2] + \lambda_4 \Phi^\dagger \Delta \Delta^\dagger \Phi, \end{aligned} \tag{5}$$

where m_Φ and $\tilde{M}_\Delta$ are real parameters with mass dimension 2, μ is the lepton number violating parameter with positive mass dimension, and λ, λ_{1-4} are dimensionless quartic Higgs couplings. Minimization conditions for each of the scalar fields can be used to replace any two of the parameters.[4] Usually the two mass parameters m_Φ^2 and $\tilde{M}_\Delta^2$ are eliminated which leaves six independent parameters.

After transforming into the mass eigenbasis the two charged scalar fields $\Phi^\pm$ and $\Delta^\pm$ mix to the charged Higgs bosons $\chi^\pm$ and $H^\pm$ [27]. Similarly, the mixing between the two CP-odd fields (χ^0 and η^0) gives rise to ρ^0 and A. Finally, we obtain the SM Higgs field (h) and a heavy Higgs (H) by mixing the two neutral CP-even states Φ^0 and δ^0. $\chi^\pm$ and ρ^0 act as the three Goldstone bosons which give masses to the SM weak gauge bosons. The remaining seven states are the physical Higgs bosons.

The masses of the doubly and singly charged Higgs states $H^{\pm\pm}$ and $H^\pm$ are expressed in terms of the parameters in the Lagrangian as

$$m_{H^{++}}^2 = M_\Delta^2 - v_\Delta^2 \lambda_3 - \frac{\lambda_4}{2} v_\Phi^2, \tag{6}$$

$$m_{H^+}^2 = \left(M_\Delta^2 - \frac{\lambda_4}{4} v_\Phi^2\right)\left(1 + \frac{2v_\Delta^2}{v_\Phi^2}\right). \tag{7}$$

The CP-even and CP-odd neutral Higgs H, h, and A have the following masses:

$$m_h^2 = \mathcal{T}_{11}^2 \cos^2\alpha + \mathcal{T}_{22}^2 \sin^2\alpha - \mathcal{T}_{12}^2 \sin 2\alpha, \tag{8}$$

[3]The multilepton signature with triplet Higgs in a supersymmetric scenario has also been studied in [43] where singly charged Higgs decays into two gauge bosons.

[4]For the discussion on the minimization of the scalar potential, see [37].

$$m_H^2 = \mathcal{T}_{11}^2 \sin^2\alpha + \mathcal{T}_{22}^2 \cos^2\alpha + \mathcal{T}_{12}^2 \sin 2\alpha, \quad (9)$$

$$m_A^2 = M_\Delta^2 \left(1 + \frac{4v_\Delta^2}{v_\Phi^2}\right), \quad (10)$$

where $\mathcal{T}_{11}^2$, $\mathcal{T}_{22}^2$, and $\mathcal{T}_{12}^2$ are given by [27]

$$\mathcal{T}_{11}^2 = \frac{v_\Phi^2 \lambda}{2}, \quad (11)$$

$$\mathcal{T}_{22}^2 = M_\Delta^2 + 2v_\Delta^2(\lambda_2 + \lambda_3), \qquad M_\Delta^2 = \frac{v_\Phi^2 \mu}{\sqrt{2} v_\Delta}, \quad (12)$$

$$\mathcal{T}_{12}^2 = -\frac{2v_\Delta}{v_\Phi} M_\Delta^2 + v_\Phi v_\Delta (\lambda_1 + \lambda_4). \quad (13)$$

Note that the difference between $H^{\pm\pm}$ and $H^\pm$ is proportional to the coupling λ_4, i.e.

$$M_{H^\pm}^2 - M_{H^{\pm\pm}}^2 \sim \frac{\lambda_4}{2} v_\Phi^2 + \mathcal{O}(v_\Delta^2). \quad (14)$$

The Higgs triplet Δ contributes to the gauge boson masses through its vacuum expectation value v_Δ. The measurement of the ρ-parameter severely constrains the VEV to $v_\Delta \lesssim 5$ GeV [46]. Since, in our case, $v_\Delta \ll v_\Phi$, the difference between the charged Higgs masses $M_{H^{\pm\pm}}$ and $M_{H^\pm}$ is governed by the electroweak VEV v_Φ. In Fig. 1(a), we show the mass spectrum of all the Higgs states, assuming the other parameters $\lambda_1 = \lambda_2 = \lambda_3 = 1.0$, $\lambda = 0.52$, and $\lambda_4 > 0$. Note that, for our choice of parameters, the CP-odd state A and the CP-even states H are heavier than the charged Higgs states $H^\pm$, $H^{\pm\pm}$. Between the charged Higgs states, $H^\pm$ is heavier than $H^{\pm\pm}$, as $\lambda_4 > 0$. Finally, h is the SM-like Higgs boson, assumed to have a mass of 125 GeV. The other regime $\lambda_4 < 0$ gives the opposite hierarchy between the charged Higgs masses and has been explored in [27]. We show the variation of the mass spectrum of the different Higgs states with the ratio $\frac{\mu}{v_\Delta}$ in Fig. 1(b).

It is evident from Fig. 1(a) that for $\lambda_4 \lesssim \mathcal{O}(0.1)$ all the Higgs bosons are almost degenerate in masses. For larger λ_4, the charged Higgs bosons $H^\pm$, $H^{\pm\pm}$ become lighter than the neutral Higgs states H^0, A^0. Higher λ_4 (well within the perturbative regime) results in a splitting between singly charged and doubly charged Higgs masses. In the subsequent analyses, we focus on the charged Higgses with masses avoiding LEP/LHC bounds and analyze their decay widths, branching fractions, and collider signatures. Note that both the charged Higgses $H^{\pm\pm}$ and $H^\pm$ contribute to the $h \to \gamma\gamma$ process at one loop [47–49]. Very low masses can cause deviation in the measured signal strength $\mu_{\gamma\gamma}$ at the LHC [50]. Since no direct bound exists from LHC on these masses for $v_\Delta \gtrsim 10^{-5}$ GeV, it might, therefore, be possible to set a lower bound on the masses of charged scalars from the observed value of the diphoton signal strength. As mentioned in [49], the lower bounds on the charged scalar masses can be considered as $m_{H^\pm} \sim 130$ GeV and $m_{H^{\pm\pm}} \sim 100$ GeV allowing 2σ deviation from the central values of the T-parameter and observed diphoton signal strength.

III. DECAY WIDTHS AND BRANCHING RATIOS

As outlined in the previous section, we consider a mass spectrum, where the singly charged Higgs is heavier than the doubly charged Higgs, $M_{H^+} > M_{H^{++}}$. The doubly charged Higgs $H^{\pm\pm}$ has only a limited number of decay modes, i.e. decays into same-sign dileptons and same-sign dibosons. The partial decay widths of the dileptonic channel depends on the strength of the corresponding Yukawa coupling $Y_\Delta \sim \frac{M_\nu}{v_\Delta}$. For small $v_\Delta \sim 10^{-9}$ GeV, this

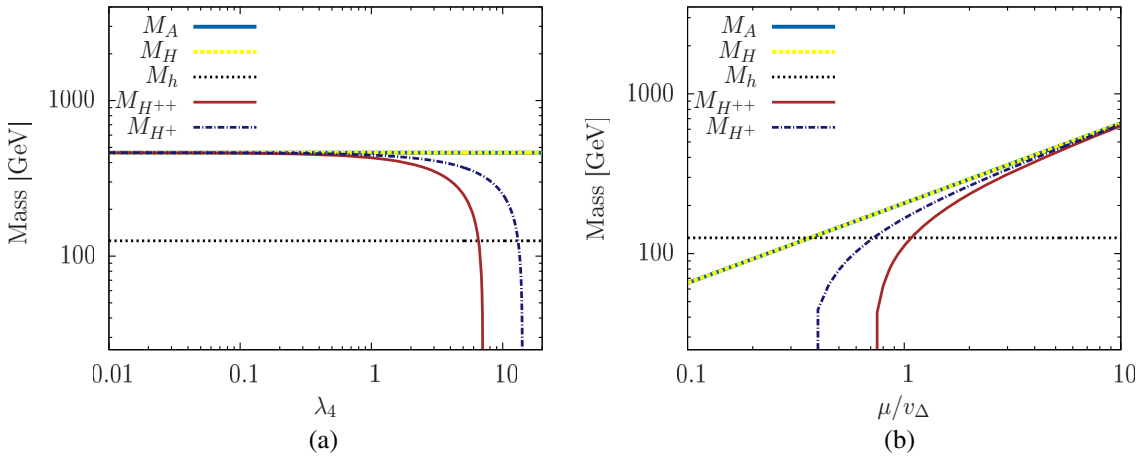

FIG. 1. Variation of the masses of the Higgs states with the coupling λ_4 (left panel) and with μ/v_Δ (right panel). The other parameters have been set to $\lambda_{1,2,3} = 1.0$, $\lambda = 0.52$, and $v_\Delta = 10^{-5}$ GeV. For the figure in the left panel, $\mu = 5 \times 10^{-5}$ GeV, and for the right panel $\lambda_4 = 1.0$. The mass of the SM Higgs is 125 GeV.

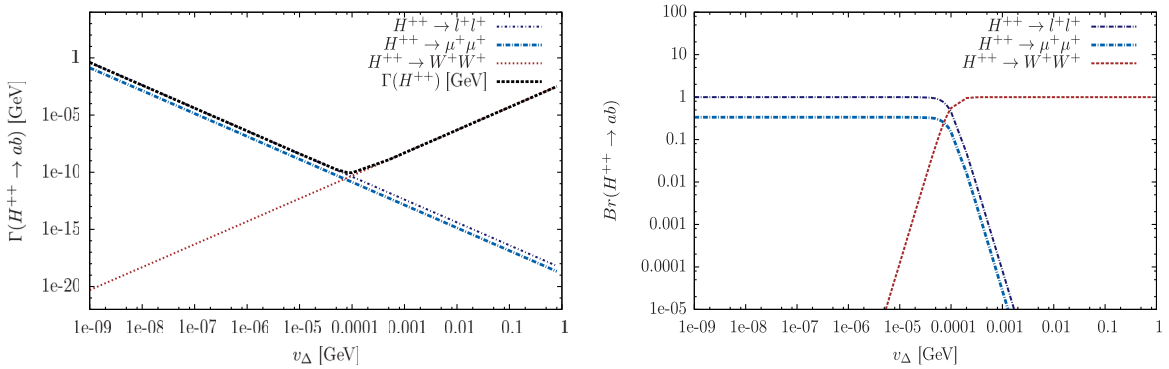

FIG. 2. Partial decay widths (left panel) and branching ratios (right panel) of the doubly charged Higgs H^{++} into different final states. The dark (light) blue dot-dashed line represent the branching ratio of $H^{++} \to l^+l^+(\mu^+\mu^+)$ states. The red dashed line represents BR $(H^{++} \to W^+W^+)$. The masses of the Higgs triplet is $M_{H^{++}} = 630$ GeV. The total width is denoted by the black line.

gives rise to large coupling strength $Y_\Delta \sim \mathcal{O}(1)$ and hence, a large partial width. The bosonic decay mode $H^{\pm\pm} \to W^\pm W^\pm$ is, on the other hand, proportional to the v_Δ^2. Therefore, the partial width (and, also the branching ratio) for this channel becomes large for a large v_Δ [23,24].

With the choice for our mass spectrum, $H^{\pm\pm} \to H^\pm W^\pm$ remains absent. We show the decay widths and branching ratios in Fig. 2, for the illustrative mass point $M_{H^{++}} \simeq$ 630 GeV. This value is in agreement with current limits from ATLAS [38]. The variation of the decay width and branching fractions with the doubly charged Higgs mass is nominal. Hence, we do not show them explicitly. A couple of comments are in order:

(i) Leptonic final states are the dominant decay modes for smaller $v_\Delta \lesssim 10^{-4}$ GeV. For $v_\Delta \gtrsim 10^{-4}$ GeV, $H^{++} \to W^+W^+$ becomes dominant, as evident from Fig. 2, exceeding $H^{++} \to l^+l^+$ [23].

(ii) The decay widths and the branching ratio of $H^{++} \to l^+l^+$ depends on the neutrino oscillation parameters θ_{12}, θ_{23}, θ_{13}, the light neutrino masses m_i, and the CP violating phases. In our analysis we consider the best fit value of the oscillation parameters [1], $\theta_{12} = 33.48°, \theta_{13} = 8.50°, \theta_{23} = 42.4°$, and the light neutrino masses $m_1 = 0.10$ eV, $m_2 = 0.100376$ eV, and $m_3 = 0.110589$ eV. We choose the CP phases to be zero. In Fig. 2, the leptonic mode involves all three leptons e, μ, τ, and we separately show the $\mu\mu$ channel.

(iii) The branching ratio of $H^{\pm\pm} \to \mu^\pm\mu^\pm$ is 31.5% for small $v_\Delta \lesssim 10^{-5}$ GeV. The branching ratio to ee and $\tau\tau$ are also comparable, while the $e\mu$, $e\tau$, and other off-diagonal branching ratios are relatively smaller.

The singly charged Higgs, on the other hand, can decay to a number of final states, including $l^+\nu$, W^+Z, W^+h, W^+H^{++}, and $t\bar{b}$. For $M_{H^+} - M_{H^{++}} < M_{W^+}$, H^+ will also decay via the off-shell mode $H^{++}W^{-*}$. We show the branching ratios of the different decay modes in Fig. 3 for the scenario $M_{H^+} - M_{H^{++}} < M_W$. It is evident from the left panel that for $v_\Delta < 10^{-7}$ GeV, the leptonic mode $H^+ \to l^+\nu$ $(l = e, \mu, \tau)$ is the dominant decay channel. In the intermediate range of $v_\Delta \sim 10^{-6}$–10^{-2} GeV, $H^+ \to H^{++}W^{-*} \to H^{++}jj + l\nu$ is maximized. A similar feature of the branching ratios is present for the on-shell mode $H^+ \to H^{++}W^-$. Interestingly, for this case, the above mode remains dominant even for much lower values of $v_\Delta \sim 10^{-8}$ GeV. Note that, although we have only shown the branching ratios for a few illustrative mass points of H^+ and H^{++}, the features remain unaltered for other masses as well. This intermediate v_Δ region is of particular interest, as the decay mode $H^+ \to H^{++}W^-/H^{++}W^{-*}$ can give distinctive multilepton signatures (with five/six leptons in the final state) at the LHC (and VLHC). We will explore this in detail in Sec. V B.

IV. PRODUCTION CROSS SECTION AT LHC AND VLHC

In this section we discuss the production of the charged Higgs boson states at the LHC at 13 TeV and the VLHC with center-of-mass energy of 100 TeV. The dominant

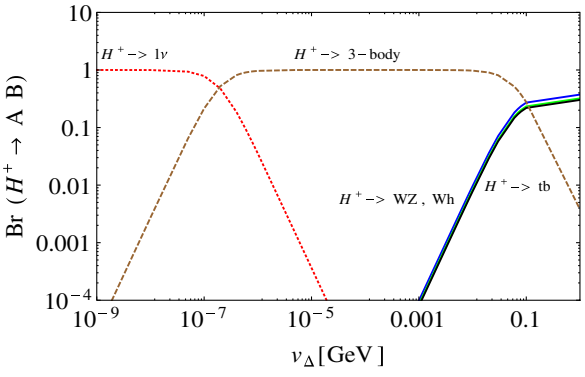

FIG. 3. Branching ratios of the different decay modes of H^+, for the illustrative mass point, $M_H^+ = 445$ GeV, $M_H^{++} = 428$ GeV.

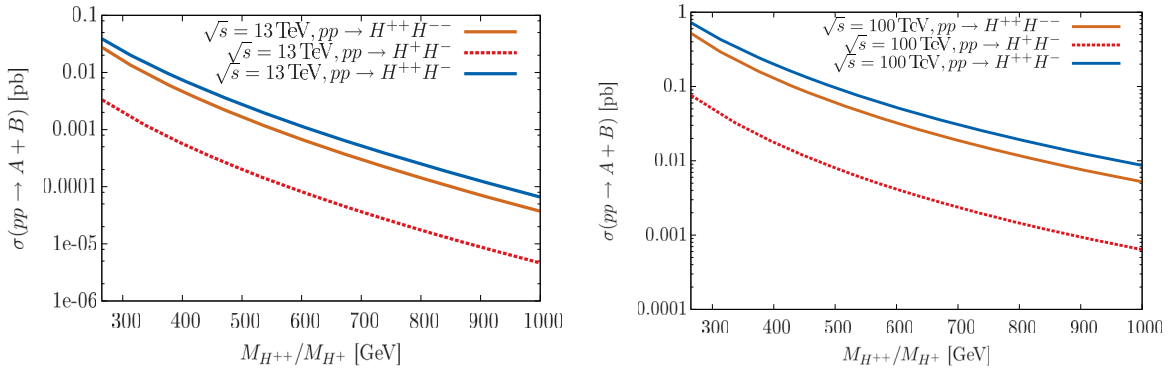

FIG. 4. Variation of the production cross section of charged Higgs with mass. Left panel: 13 TeV; right panel: 100 TeV. The K-factor for 13 TeV has been chosen as 1.25 [29].

processes are the pair production of $H^{\pm\pm}/H^{\pm}$ through the s-channel Z/γ exchange and the associated production of singly and doubly charged Higgs bosons, i.e. $pp \to H^{\pm\pm}H^{\mp}$, mediated by the W boson.

We use FeynRules [51] to generate a suitable model file via Universal Feynrules Output (UFO) [52,53] interface and compute the hard process with MadGraph5_aMC@NLO [54]. Eventually, the generated events are showered and hadronized using Pythia [55,56]. To mimic the detector response, a fast detector simulation is performed using Delphes-3.3 [57]. All cross sections have been evaluated with NN23LO1 [58] as a parton distribution function. We show the production cross section for the processes $pp \to H^{++}H^{--}$, $pp \to H^{+}H^{--} + \text{H.c.}$, and $H^{+}H^{-}$ in Figs. 4(a) and 4(b) for the center-of-mass (c.o.m.) energies $\sqrt{s} = 13$ and 100 TeV, respectively. For the 13 TeV c.o.m. energy we multiply the lowest order (LO) cross section by the K-factor $K = 1.25$ [29]. As mentioned earlier, the production of $H^{++}H^{-}$ and $H^{--}H^{+}$ provide the largest cross sections among all channels. Because of their electromagnetic charge, the cross section of pair produced doubly charged Higgs bosons is large compared to singly charged Higgs pair production.

V. MULTILEPTON SIGNATURE AT LHC AND VLHC

A large number of final states can arise from the pair production of doubly or singly charged Higgs bosons. ATLAS has performed searches for doubly charged Higgs bosons in the same-sign dielectron channel for $\sqrt{s} =$ 13 TeV with 13.9 fb^{-1} of data [38]. Assuming a 100% branching ratio of $H^{\pm\pm} \to e^{\pm}e^{\pm}$, a lower bound on the doubly charged Higgs mass is obtained, $M_{H^{++}} \geq 570$ GeV. However, depending on the parameter space, this limit can be relaxed due to the presence of other decay modes. For illustration, we consider a scenario where $v_\Delta \sim 10^{-9}$ GeV resulting in $\text{BR}(H^{++} \to e^{+}e^{+}) = 0.315$. The bound on the mass of doubly charged Higgs bosons becomes significantly weaker, as shown in Fig. 5. The red line corresponds to the theory prediction from [38]. The limit on $M_{H^{++}}$ remains mostly unchanged as the branching ratio of the H^{++} decaying into leptons is largely constant for $v_\Delta \lesssim 10^{-5}$ GeV [see Fig. 2(b)]. Instead, for larger $v_\Delta \gtrsim 10^{-5}$ GeV, the branching ratio into leptonic final states is even more suppressed, as the other modes, i.e. decays into gauge bosons, start to dominate and, hence, the limit becomes irrelevant. Another bound presented by CMS for the $H^{++}jj$ channel can only constrain the triplet VEV $v_\Delta \geq 16$ GeV [39] which is out of our region of interest.

Below, we consider three separate regions for the triplet VEV, namely low, intermediate, and large, and we discuss various multilepton signatures relevant for each.

A. Small v_Δ ($\leq 10^{-6}$ GeV)

The most promising channel for small v_Δ is the search for pair produced H^{++} decaying into dilepton. Hence, the final state consists of 4 leptons. We show the variation of

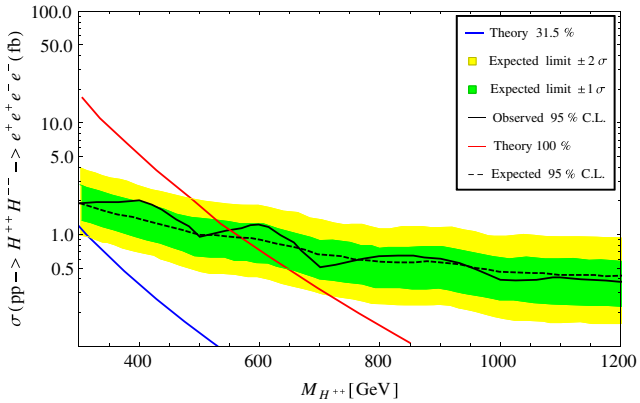

FIG. 5. The limit on the cross section folded with branching ratios from 13 TeV LHC results [38]. The blue line represents the limit for our scenario with $v_\Delta = 10^{-9}$ GeV, where the branching ratio of $H^{++} \to e^{+}e^{+}$ is 0.315. The K-factor for the 13 TeV limit has been taken as 1.25 [29].

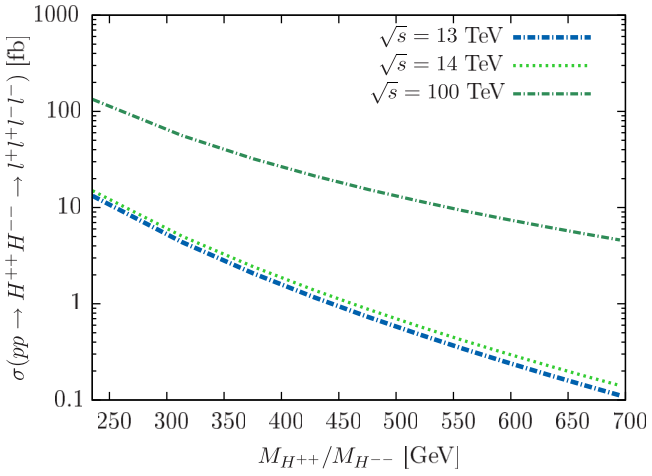

FIG. 6. The cross section for $4l$ for 13, 14, and 100 TeV c.o.m. energy. The K-factor for 13 TeV limit has been taken as 1.25 [29].

the cross section of $pp \to H^{++}H^{--} \to 4l$ with $m_{H^{\pm\pm}}$ for different c.o.m. energies $\sqrt{s} = 13$, 14, and 100 TeV in Fig. 6. For the 13 TeV c.o.m. energy the cross section is greater than 1 fb up to mass $M_{H^{\pm\pm}} \sim 450$ GeV. We perform a detailed signal and background analysis for the 4l case at 13 TeV c.o.m. energy at the LHC. We also show the results for 100 TeV c.o.m. energy relevant for the VLHC.

Analysis: We consider two benchmark scenarios, a low and a high mass doubly charged Higgs boson, both in agreement with the present bound from the LHC (see Fig. 5):

(i) $M_{H^{++}} = 375$ GeV, obtained from $v_\Delta = 10^{-9}$ GeV and $\mu = 4 \times 10^{-9}$ GeV.
(ii) $M_{H^{++}} = 630$ GeV with $v_\Delta = 10^{-9}$ GeV and $\mu = 10^{-8}$ GeV.

We generate the 4l background which arises predominantly through SM diboson production. In Fig. 7 we show the distribution of various variables before cuts. Figure 7(a) describes the p_T of the hardest final state lepton. The invariant mass of the two positively charged leptons $M_{l^+l^+}$ is shown in Fig. 7(b). We use the following isolation and selection criteria for the final state leptons ($e^\pm$ and $\mu^\pm$):

(i) $|\eta| < 2.5$ and $p_{T,l} > 20$ GeV.
(ii) To avoid any contamination from jet fakes, we require the hadronic activity within a cone $\Delta R = 0.4$ around an isolated lepton to be $p_{T,\text{had}} \leq 0.15 p_{T,l}$.

We apply a series of analysis cuts in order to improve the separation of signal and background:

(i) a strict p_T requirement for the hardest lepton: $p_{T,l_1} > 100$ GeV.
(ii) invariant mass of the same-sign lepton pair: $|M_{l^+l^+} - M_{H^{++}}| \leq 100$ GeV.
(iii) veto events with invariant mass around the Z peak: $|M_{l^+l^-} - M_Z| \leq 10$ GeV.

The cross sections after analysis cuts are given in Table I for the two illustrative mass points. For the lower charged Higgs mass of 375 GeV, the cross section before and after cuts are 1.659 fb and 0.827 fb, respectively. For the higher mass 630 GeV the cross sections are 0.149 fb and 0.074 fb. In addition, we also investigate the above channel for the 100 TeV collider, where the cross section increases by a factor of 30.

The inclusive partonic cross section for the SM background at 13 TeV is ~51 fb, and thus is much larger than the signal cross section. However, the dilepton invariant mass cut along with the Z veto are extremely helpful to reject the background. We compute the statistical significance of this channel as

$$n = \frac{\mathcal{S}}{\sqrt{\mathcal{S} + \mathcal{B}}}, \tag{15}$$

where $\mathcal{S}$ and $\mathcal{B}$ represent the number of signal and background events. We find that

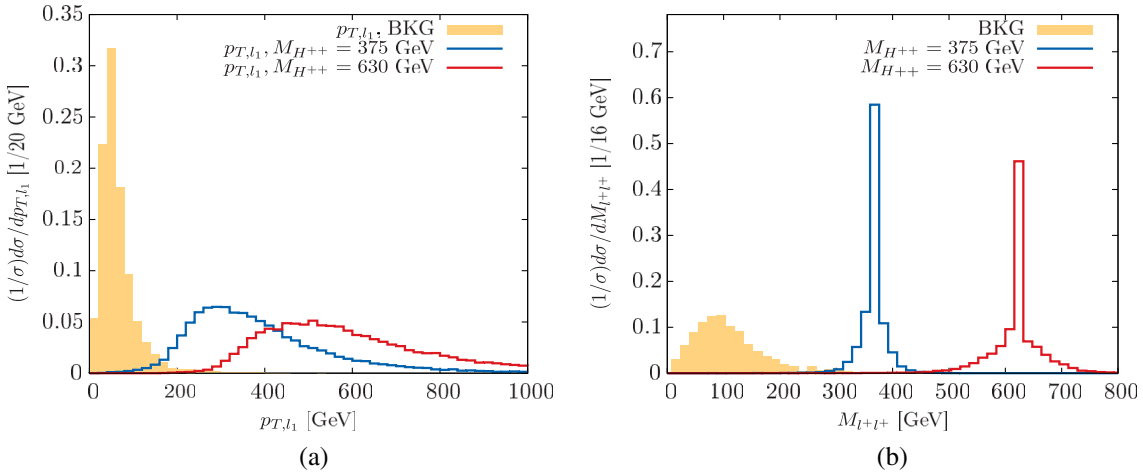

FIG. 7. (a) p_T distribution of the leading lepton. (b) Invariant mass distribution of two same-sign leptons. Both distributions correspond to the scenario $v_\Delta = 10^{-9}$ GeV. The solid curve is for the SM background.

TABLE I. The cross sections and the number of events after the final selection cuts for the channel $pp \to H^{++}H^{--} \to l^+l^+l^-l^-$, where $l = e, \mu$. The vacuum expectation value of Higgs triplet $v_\Delta = 10^{-9}$ GeV. The number of events for both 13 TeV and 100 TeV c.o.m. energy have been computed with 300 and 30 fb^{-1} luminosity. In the high luminosity run of 13 TeV LHC at 3000 fb^{-1}, the number of observed events may increase one order higher than the numbers in column four.

$\sqrt{s} = 13$ TeV						
	$pp \to H^{++}H^{--} \to l^+l^+l^-l^-$			Background $pp \to 4l$		
Masses (GeV)	Cross section before cuts [fb]	Cross section after cuts [fb]	Number of events	Cross section before cuts [fb]	Cross section after cuts [fb]	Number of events
375	1.659	0.827	248	51.12	0.0107	3
630	0.149	0.074	22	51.12	0.0015	∼0
$\sqrt{s} = 100$ TeV and $\mathcal{L} = 30$ fb^{-1}						
	$pp \to H^{++}H^{--} \to l^+l^+l^-l^-$			Background $pp \to 4l$		
Masses (GeV)	Cross section before cuts [fb]	Cross section after cuts [fb]	Number of events	Cross section before cuts [fb]	Cross section after cuts [fb]	Number of events
375	32.16	7.66	229	335.1	0.057	1
630	6.317	1.415	42	335.1	6.7×10^{-3}	∼0

(i) The doubly charged Higgs boson of mass $M_{H^{++}} = 375$ GeV can be discovered at the LHC with 300 fb^{-1} luminosity with more than 5σ significance, while for the higher mass of 630 GeV, the significance is around 4.66σ with the same amount of data.
(ii) A heavier doubly charged Higgs of mass 630 GeV can be discovered at HL-LHC (13 TeV) or VLHC (30 fb^{-1}) with more than 5σ significance.

B. Intermediate v_Δ (10^{-6}–10^{-2} GeV)

In this region, H^+ preferably decays into, either on-shell or off-shell, $H^{++}W^-$, depending on the mass splitting between the two Higgs states. H^{++} subsequently decays either into two leptons or into two W bosons. The branching fraction into gauge bosons, i.e. $H^{++} \to W^+W^+$, becomes dominant for $v_\Delta > 10^{-4}$ GeV. This intermediate range of v_Δ allows for signatures with five (or even six) leptons. Below, we discuss two channels with four and five leptons in the final states:

(i) $pp \to H^{\pm\pm}H^\mp$, subsequently $H^\mp \to W^{\pm *}H^{\mp\mp}/W^+H^{\mp\mp} \to 5W \to 5l + \not{E}_T$.
(ii) $pp \to H^{\pm\pm}H^\mp$, subsequently $H^\mp \to W^{\pm *}H^{\mp\mp}/W^\pm H^{\mp\mp} \to 5W \to 4l + 2j + \not{E}_T$.

The large lepton multiplicity reduces the cross section, but results in a cleaner (i.e. background free) signal. The parton level cross section for $4W + l + \not{E}_T$ is shown in Fig. 8. We adopt the following criteria for the leptons and jets reconstruction:

(i) $|\eta_l| < 2.5$ and $p_{T,l} > 20$ GeV and hadronic activity around an isolated lepton within a cone of $\Delta R = 0.4$ has to be $p_{T,\text{had}} \leq 0.15 p_{T,l}$.
(ii) $|\eta_j| < 4.7$ and $p_{T,j} > 30$ GeV.

In Table II, we show the cross sections for the above channels assuming on-shell decays only. Again, we consider two benchmark points with masses $M_{H^{++}} = 223$ (169) GeV and $M_{H^+} = 332$ (298) GeV. In order to obtain large enough mass splittings for decays into on-shell W, λ_4 needs to be tuned to values $\sim\mathcal{O}(1)$.

We find that the final state with five leptons occurs only in a handful of events for an integrated luminosity of 300 fb^{-1} at the LHC. As these processes are limited only by their rate, the HL-LHC provides a promising environment. The main contribution for the five-leptonic states comes from triple gauge boson production with a cross section of ∼0.025 fb. Hence, we do not analyze the background for the 5l channel.

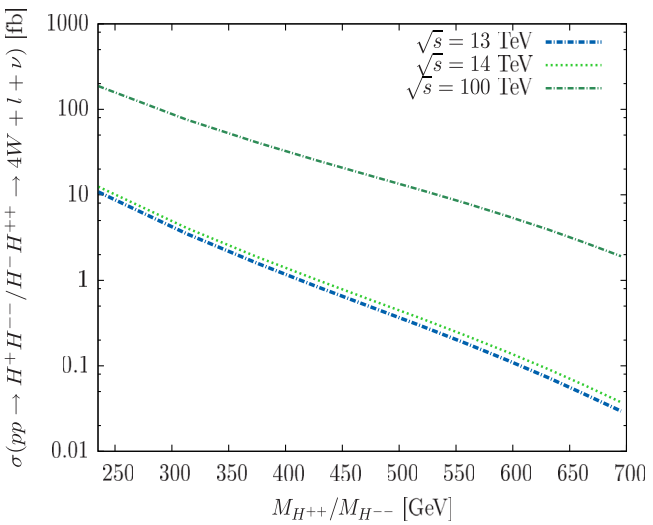

FIG. 8. Cross section for the $pp \to H^+H^{--} \to 4W + l + \not{E}_T$ channel via cascade (i.e. off-shell or on-shell W) decay of $H^+ \to H^{++}l\not{E}_T$ for $v_\Delta = 10^{-2}$ GeV. The conjugate channel is also included. For the 13 and 14 TeV, we consider a K-factor $K = 1.25$ [29].

TABLE II. The cross sections before and after cuts for the channel $pp \to H^{\pm\pm}H^{\mp} \to H^{\pm\pm}H^{\mp\mp}W^{\pm} \to 5W$ with H^{+} decaying to on-shell W. Demanding W to decay into leptonic or hadronic mode gives two different final states. (a) All leptonic: $(5l + E_T)$, and (b) 1 Hadronic: $(4l + 2j + E_T)$. The vacuum expectation value of Higgs triplet $v_\Delta = 10^{-3}$ GeV. The number of events have been computed with 300 fb^{-1} and 3000 fb^{-1} for $\sqrt{s} = 13$ TeV at the LHC. See text for further details.

$\sqrt{s} = 13$ TeV				
Channel	$M_{H^{++}}$, $M_{H^{+}}$ [GeV]	$\sigma_{\text{before cuts}}$ [fb]	$\sigma_{\text{after cuts}}$ [fb]	No. of events at (300, 3000) fb^{-1}
$(5l + E_T)$	(169, 298)	0.024	0.0054	2, 16
	(223, 332)	0.0124	0.0034	1, 10
$(4l + 2j + E_T)$	(169, 298)	0.076	0.036	10, 107
	(223, 332)	0.0393	0.016	5, 47

The dominant background for $4l + \text{jets} + \not{E}_T$ is $t\bar{t}Z$ with $\sigma(t\bar{t}Z) \simeq 586.4$ fb. After applying a Z veto cut, the remaining cross section is reduced to a manageable rate of 0.094 fb. After all cuts we find a signal cross section of 0.036 fb for the masses $M_H^{++} = 169$ GeV and $M_{H^+} = 298$ GeV. The signal for the above masses can be probed with a significance of 5.45σ with 3000 fb^{-1} and 1.73σ for 300 fb^{-1}, respectively.

C. Large v_Δ ($> 10^{-2}$ GeV)

In the large v_Δ region ($\geq 10^{-2}$ GeV), the branching ratio of $H^{\pm\pm} \to W^{\pm}W^{\pm}$ is enhanced (see Fig. 2). We consider pair production of $H^{++}H^{--}$ where subsequent decays of the gauge bosons into leptons gives rise to the $4l + E_T$ signature. This has recently been analyzed in the nonminimal composite Higgs scenario [59]. Note that this decay mode $H^{\pm\pm} \to W^{\pm}W^{\pm}$ is very poorly constrained by LHC searches [39] and a lighter doubly charged Higgs is not yet ruled out.

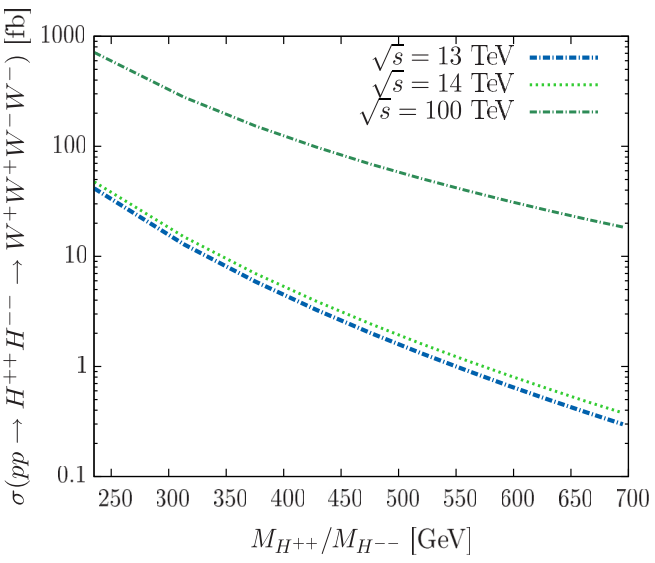

FIG. 9. Cross section for the $pp \to H^{++}H^{--} \to 4W$ against varying mass for fixed $v_\Delta = 1$ GeV. For the 13 (14) TeV c.o.m. energy, we consider $K = 1.25$.

We consider $v_\Delta = 1$ GeV and $M_{H^{++}}$ as low as 235 GeV for this analysis. We show the production cross section for the process $pp \to H^{++}H^{--} \to 4W$ in Fig. 9.

The cross section of the fully leptonic channel at 13 TeV is too small. Hence, we focus on higher c.o.m. energy $\sqrt{s} = 100$ TeV. This channel can also produce a combination of leptonic and hadronic final states which will not be considered here. We estimate the following SM processes as backgrounds:

(i) $pp \to 4lZ$ and $Z \to \nu\nu$.
(ii) $pp \to 4lW$ with subsequent decays of $W \to l\nu$ (with a lepton escaping detection).
(iii) $pp \to 2lWW$ with subsequent decays of $W \to l\nu$.

In addition to the above processes, we also consider the $t\bar{t}Z$ process followed by the further decays of $t \to bW$ and $Z \to l^{+}l^{-}$ that can generate $4l + E_T$ associated with b-jets. Note that the b-jet from the above mentioned background has large p_T. Hence, in spite of a large cross section, most of these background events can be rejected applying jet and Z veto.

In the signal, the $H^{\pm\pm}$ decay into a pair of $W^{\pm}$ bosons which subsequently decay into leptons; hence, final states

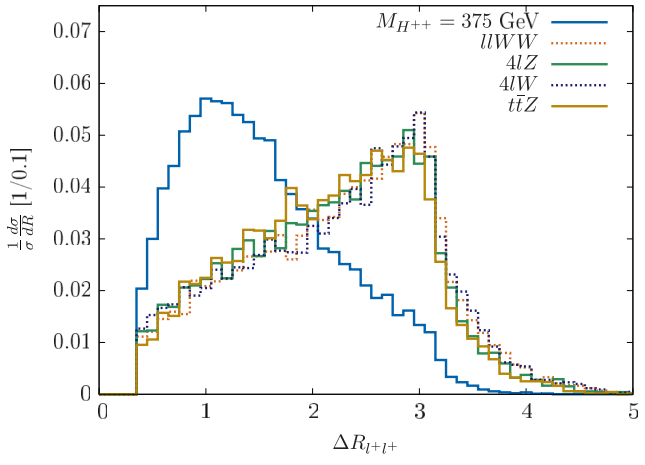

FIG. 10. ΔR distribution for two same sign leptons for the process $pp \to 4l + E_T$ assuming $v_\Delta = 1$ GeV. The center-of-mass energy is $\sqrt{s} = 100$ TeV.

TABLE III. The cross sections at 100 TeV collider after basic trigger cut and selection cuts for the channel $pp \to H^{++}H^{--} \to W^+W^+W^-W^- \to 4l + E_T$, where $l = e, \mu$. The vacuum expectation value of Higgs triplet $v_\Delta = 1$ GeV. The number of events have been computed with the aim of achieving 300 fb^{-1} luminosity.

$\sqrt{s} = 100$ TeV				
Channel	$M_{H^{++}}$ [GeV]	$\sigma_{\text{before cuts}}$ [fb]	$\sigma_{\text{after cuts}}$ [fb]	No. of events at 300 fb^{-1}
$pp \to H^{++}H^{--} \to 2W^+2W^-$	235 GeV	0.643	0.355	106
$\to 4l + E_T$	375 GeV	0.155	0.093	27
Background				
$pp \to 4lZ$, $Z \to \nu\nu$	⋯	0.291	0.0068	2
$pp \to 2lW^+W^-$, $W \to l\nu$	⋯	3.12	0.097	29
$pp \to 4lW$, $W \to l\nu$	⋯	0.31	0.0073	2
$pp \to t\bar{t}Z \to 4l + 2b + E_T$	⋯	48.51	0.0165	4

are collimated in the lab frame and populate the same hemisphere in the detector (see Fig. 10). Such configurations are much less likely in SM processes. We exploit this by applying a cut on the ΔR separation of the same-sign dilepton system. We demand four leptons in the final state and employ the following sets of analysis cuts:

(i) veto events with jet leading jet $p_T > 40$ GeV,
(ii) $\Delta R < 2.0$ between two same-sign leptons,
(iii) veto events with $|M_{l^+l^-} - M_Z| < 10$ GeV.

The cross sections are shown in Table III for two illustrative mass points $M_{H^{++}} = 235$ and 375 GeV. We find that the above mass points can be discovered at a VLHC with the following significance:

$$\frac{\mathcal{S}}{\sqrt{\mathcal{S}+\mathcal{B}}} = 8.87\sigma(3.37\sigma) \quad \text{for } M_{H^{\pm\pm}} = 235\,(375)\text{ GeV}. \tag{16}$$

VI. CONCLUSION

We investigated various multilepton signatures that arise in a Type II seesaw model with a Higgs triplet. The model contains singly charged Higgs bosons as well as doubly charged Higgs states. Depending on the triplet scalar VEV v_Δ, H^{++} and H^+ can have a number of decay modes. We focus on three different regimes of v_Δ and investigate the multilepton final states for each different regime. For small v_Δ ($< 10^{-6}$ GeV), H^{++} prefers to decay to two same-sign leptons. Therefore, pair production of $H^{++}H^{--}$ leads to a distinctive four leptonic signature. Assuming 100% branching ratios of $H^{++} \to l^+l^+$, the recent LHC search has constrained $M_{H^{++}} > 570$ GeV. However, the limit is considerably weakened for a parameter space with a lower branching ratio to leptons. We discuss in detail the prospects to observe this mode at the current run of the LHC and also at a future hadron collider to be run at a c.o.m. energy of 100 TeV. We summarize our observations as follows:

(i) The channel with four leptons, arising from $H^{\pm\pm}$ decays, offers the most promising signature for small v_Δ. We conclude that a doubly charged Higgs boson of mass 375 GeV can be discovered at 13 TeV LHC with 300 fb^{-1} luminosity. Higher mass range 630 GeV can further be discovered at a high-luminosity LHC or at a VLHC with 30 fb^{-1} luminosity.
(ii) For the intermediate v_Δ range, the most distinctive channel arises from cascade decays of the singly charged Higgs $H^+ \to H^{++}W^-$ (both on-shell and off-shell). Further, H^{++} can decay in either dilepton or W^+W^+ modes. This leads to a final state consisting of $5W$. If all W decay leptonically, rates are very small, resulting in ∼ tens of events for 300 fb^{-1} luminosity at 13 TeV. But the signal is very clean. We also analyze another topology with $4l+2j+E_T$. SM backgrounds for these channels are extremely small which makes it an interesting search strategy. A lighter doubly charged Higgs mass around 169 GeV can be conclusively discovered with more than 5σ at a high luminosity run of LHC.
(iii) Finally, the large v_Δ region, which is poorly constrained at the LHC, seems to be the most promising channel to probe lighter doubly charged Higgs bosons at the VLHC. In this case, the four leptons in the final state appear from the pair production of $H^{++}H^{--}$ followed by the decay of $H^{\pm\pm} \to W^\pm W^\pm$. We find that a doubly charged Higgs of mass 235 GeV can be discovered at $\sim 8\sigma$ significance at the VLHC.

The properties of the SM-like Higgs boson has been quite well established by the LHC. No new physics has been observed so far, barring some initial statistical fluctuations, fuelling hope for potential signals. Many of the new physics models, although proposed long ago, lack detailed studies covering all their parameter regions. We explored parts of the parameter space of a SM extension with a Higgs triplet which is, otherwise, difficult to probe at existing (and future) colliders. Finding a (doubly) charged

Higgs boson will be an immediate proof for the existence of at least another $SU(2)_L$ scalar multiplet.

ACKNOWLEDGMENTS

The work of M. M. has been supported by the Royal Society International Exchange Program and DST-INSPIRE-15-0074 grant. M. M. thanks IPPP, Durham University, UK for hospitality where part of the work was being carried out. S. N. acknowledges Dr. D. S. Kothari Post Doctoral Fellowship (Award No. PH/15-16/0073) awarded by University Grant Commission (UGC), India for financial support. M. M. and S. N. thank Dr. Shankha Banerjee and Prof. C. Lester for their invaluable inputs and Dr. Santosh Kumar Rai for providing the FeynRules model file.

[1] M. C. Gonzalez-Garcia, M. Maltoni, and T. Schwetz, Nucl. Phys. **B908**, 199 (2016).
[2] P. A. R. Ade *et al.* (Planck Collaboration), Astron. Astrophys. **594**, A13 (2016).
[3] S. Weinberg, Phys. Rev. Lett. **43**, 1566 (1979).
[4] F. Wilczek and A. Zee, Phys. Rev. Lett. **43**, 1571 (1979).
[5] P. Minkowski, Phys. Lett. **67B**, 421 (1977).
[6] R. N. Mohapatra and G. Senjanovic, Phys. Rev. Lett. **44**, 912 (1980).
[7] T. Yanagida, Conf. Proc. C **7902131**, 95 (1979).
[8] M. Gell-Mann, P. Ramond, and R. Slansky, Conf. Proc. C **790927**, 315 (1979).
[9] J. Schechter and J. W. F. Valle, Phys. Rev. D **22**, 2227 (1980).
[10] R. E. Shrock, Phys. Rev. D **24**, 1232 (1981).
[11] M. Magg and C. Wetterich, Phys. Lett. **94B**, 61 (1980).
[12] T. P. Cheng and L. F. Li, Phys. Rev. D **22**, 2860 (1980).
[13] G. Lazarides, Q. Shafi, and C. Wetterich, Nucl. Phys. **B181**, 287 (1981).
[14] R. N. Mohapatra and G. Senjanovic, Phys. Rev. D **23**, 165 (1981).
[15] R. Foot, H. Lew, X. G. He, and G. C. Joshi, Z. Phys. C **44**, 441 (1989).
[16] J. C. Pati and A. Salam, Phys. Rev. D **10**, 275 (1974); R. N. Mohapatra and J. C. Pati, Phys. Rev. D **11**, 566 (1975); **11**, 2558 (1975); G. Senjanović and R. N. Mohapatra, Phys. Rev. D **12**, 1502 (1975).
[17] R. N. Mohapatra, Phys. Rev. Lett. **56**, 561 (1986); R. N. Mohapatra and J. W. F. Valle, Phys. Rev. D **34**, 1642 (1986); D. Wyler and L. Wolfenstein, Nucl. Phys. **B218**, 205 (1983); E. Witten, Nucl. Phys. **B268**, 79 (1986); J. L. Hewett and T. G. Rizzo, Phys. Rep. **183**, 193 (1989).
[18] P. S. B. Dev and R. N. Mohapatra, Phys. Rev. D **81**, 013001 (2010); S. Blanchet, P. S. B. Dev, and R. N. Mohapatra, Phys. Rev. D **82**, 115025 (2010).
[19] M. C. Chen and J. Huang, Mod. Phys. Lett. A **26**, 1147 (2011).
[20] W.-Y. Keung and G. Senjanović, Phys. Rev. Lett. **50**, 1427 (1983).
[21] C. Y. Chen, P. S. B. Dev, and R. N. Mohapatra, Phys. Rev. D **88**, 033014 (2013); P. S. B. Dev, R. N. Mohapatra, and Y. Zhang, J. High Energy Phys. 05 (2016) 174.
[22] M. Mitra, R. Ruiz, D. J. Scott, and M. Spannowsky, Phys. Rev. D **94**, 095016 (2016).
[23] P. Fileviez Perez, T. Han, G. y. Huang, T. Li, and K. Wang, Phys. Rev. D **78**, 015018 (2008).
[24] A. Melfo, M. Nemevsek, F. Nesti, G. Senjanovic, and Y. Zhang, Phys. Rev. D **85**, 055018 (2012).
[25] F. del Aguila and J. A. Aguilar-Saavedra, Nucl. Phys. **B813**, 22 (2009).
[26] S. Chakrabarti, D. Choudhury, R. M. Godbole, and B. Mukhopadhyaya, Phys. Lett. B **434**, 347 (1998).
[27] M. Aoki, S. Kanemura, and K. Yagyu, Phys. Rev. D **85**, 055007 (2012).
[28] E. J. Chun and P. Sharma, Phys. Lett. B **728**, 256 (2014).
[29] A. G. Akeroyd and M. Aoki, Phys. Rev. D **72**, 035011 (2005).
[30] S. Banerjee, M. Frank, and S. K. Rai, Phys. Rev. D **89**, 075005 (2014).
[31] P. S. Bhupal Dev, D. K. Ghosh, N. Okada, and I. Saha, J. High Energy Phys. 03 (2013) 150; 05 (2013) 049(E).
[32] F. del Aguila and M. Chala, J. High Energy Phys. 03 (2014) 027.
[33] F. del Aguila, M. Chala, A. Santamaria, and J. Wudka, Acta Phys. Pol. B **44**, 2139 (2013).
[34] M. Lindner, M. Platscher, and F. S. Queiroz, arXiv: 1610.06587.
[35] M. Mitra, G. Senjanovic, and F. Vissani, Nucl. Phys. **B856**, 26 (2012).
[36] M. Muhlleitner and M. Spira, Phys. Rev. D **68**, 117701 (2003).
[37] A. Arhrib, R. Benbrik, M. Chabab, G. Moultaka, M. C. Peyranere, L. Rahili, and J. Ramadan, Phys. Rev. D **84**, 095005 (2011).
[38] ATLAS Collaboration, Report No. ATLAS-CONF-2015-051.
[39] V. Khachatryan *et al.* (CMS Collaboration), Phys. Rev. Lett. **114**, 051801 (2015).
[40] S. Kanemura, K. Yagyu, and H. Yokoya, Phys. Lett. B **726**, 316 (2013).
[41] S. Kanemura, M. Kikuchi, K. Yagyu, and H. Yokoya, Phys. Rev. D **90**, 115018 (2014).
[42] S. Kanemura, M. Kikuchi, H. Yokoya, and K. Yagyu, Prog. Theor. Exp. Phys. **2015**, 051B02 (2015).
[43] P. Bandyopadhyay, K. Huitu, and A. Sabanci Keceli, J. High Energy Phys. 05 (2015) 026.
[44] N. Arkani-Hamed, T. Han, M. Mangano, and L. T. Wang, Phys. Rep. **652**, 1 (2016).
[45] T. Golling *et al.*, arXiv:1606.00947.

[46] S. Kanemura and K. Yagyu, Phys. Rev. D **85**, 115009 (2012).
[47] A. Arhrib, R. Benbrik, M. Chabab, G. Moultaka, and L. Rahili, J. High Energy Phys. 04 (2012) 136.
[48] A. Arhrib, R. Benbrik, G. Moultaka, and L. Rahili, arXiv:1411.5645.
[49] D. Das and A. Santamaria, Phys. Rev. D **94**, 015015 (2016).
[50] ATLAS and CMS Collaborations, Report No. ATLAS-CONF-2015-051.
[51] A. Alloul, N. D. Christensen, C. Degrande, C. Duhr, and B. Fuks, Comput. Phys. Commun. **185**, 2250 (2014).
[52] C. Degrande, C. Duhr, B. Fuks, D. Grellscheid, O. Mattelaer, and T. Reiter, Comput. Phys. Commun. **183**, 1201 (2012).
[53] P. de Aquino, W. Link, F. Maltoni, O. Mattelaer, and T. Stelzer, Comput. Phys. Commun. **183**, 2254 (2012).
[54] J. Alwall, R. Frederix, S. Frixione, V. Hirschi, F. Maltoni, O. Mattelaer, H.-S. Shao, T. Stelzer, P. Torrielli, and M. Zaro, J. High Energy Phys. 07 (2014) 079.
[55] T. Sjostrand, L. Lonnblad, and S. Mrenna, arXiv:hep-ph/0108264.
[56] T. Sjostrand, S. Mrenna, and P. Z. Skands, Comput. Phys. Commun. **178**, 852 (2008).
[57] J. de Favereau, C. Delaere, P. Demin, A. Giammanco, V. Lemaître, A. Mertens, and M. Selvaggi (DELPHES 3 Collaboration), J. High Energy Phys. 02 (2014) 057.
[58] R. D. Ball, V. Bertone, S. Carrazza, L. Del Debbio, S. Forte, A. Guffanti, N. P. Hartland, and J. Rojo (NNPDF Collaboration), Nucl. Phys. **B877**, 290 (2013).
[59] C. Englert, P. Schichtel, and M. Spannowsky, arXiv:1610.07354.